A&A 454, 95–102 (2006)
DOI: 10.1051/0004-6361:20054673

Astronomy & Astrophysics

The new sample of giant radio sources

III. Statistical trends and correlations

J. Machalski and M. Jamrozy

Astronomical Observatory, Jagellonian University, ul. Orla 171, 30244 Cracow, Poland
e-mail: machalsk@oa.uj.edu.pl

Received 9 December 2005 / Accepted 28 March 2006

ABSTRACT

Aims. In this paper we analyse whether "giant" radio galaxies (GRGs) differ from "normal"-size galaxies (NSGs) except for the linear extent of their radio structure.
Methods. We compare a number of properties of GRGs with the corresponding properties of NSGs, and analyse the statistical trends and correlations of physical parameters, homogeneously determined for the sources, with their "fundamental" parameters: the redshift, radio luminosity, and linear size. Using the Pearson partial-correlation test on the correlation between two variables in the presence of one or two other variables, we examine which correlation is the strongest.
Results. The analysis clearly shows that GRGs do not form a separate class of radio sources. They most likely evolve with time from smaller sources, however under specific circumstances. Analysing properties of GRGs and NSGs together, we find that (i) the core prominence does not correlate with the total radio luminosity (as does the core power), but it anti-correlates with the surface brightness of the lobes of sources; (ii) the energy density (and possibly the internal pressure) in the lobes is independent of redshift for constant radio luminosity and size of the sources. Thus, in the analysed samples, there is no evidence for a cosmological evolution of the IGM pressure in the form $p_{\rm IGM} \propto (1+z)^5$; (iii) the equipartition magnetic-field strength, transformed into constant source luminosity and redshift, strongly correlates with the source size. We argue that this $B_{\rm eq}$–D correlation reflects a more fundamental correlation between $B_{\rm eq}$ and the source age; (iv) both the rotation and depolarisation measures suggest Faraday screens local to the lobes of sources, however their geometry and the composition of intervening material cannot be determined from the global polarisation characteristics. The significant correlation between the depolarisation measure and the linear size can be explained by less dense IGM surrounding the lobes (or cocoon) of GRGs than that in the vicinity of NSGs.

Key words. radio contiuum: galaxies – galaxies: kinematics and dynamics

1. Introduction

Classical double radio sources with projected linear size greater than 1 Mpc are commonly referred to as "giants"; this size limit was based on the cosmological constants $H_0 = 50\,{\rm km\,s^{-1}\,Mpc^{-1}}$ and $q_0 = 0.5$. After adopting a flat Universe with $H_0 = 71\,{\rm km\,s^{-1}\,Mpc^{-1}}$ and $\Omega_{\rm m} = 0.27$, the above size limit is reduced to about 700 kpc. For consistency with many previously published papers, in the present analysis we include FRII-type sources with $D \geq 700$ kpc into the sample of giants.

In Paper I (Machalski et al. 2001) we selected a sample of 36 giant radio source candidates, primarily of FRII-type morphology (Fanaroff & Riley 1974), and we presented their optical identifications and low-resolution spectra used to determine the object's redshifts. This in turn allowed us to derive a number of physical parameters for the sample sources, like projected linear size, radio luminosity, optical absolute magnitude of identified host galaxy, equipartition energy density and magnetic field strength, etc. In Paper II (Machalski et al. 2006) the previously published data were supplemented with high-frequency total-intensity and polarised-intensity radio maps, and the polarisation and depolarisation parameters of the sample sources were specified.

In this paper we compare these physical parameters determined for an enlarged sample of giant radio galaxies with the corresponding parameters in a comparison sample of normal-size FRII-type radio galaxies, i.e. samples which do not comprise quasars with extended double radio structures. Here we analyse properties of the whole radio sources. A further analysis of the sample sources' asymmetries, properties of their lobes, etc., will be given in a forthcoming paper. The observational data used is described in Sect. 2. Statistical trends and correlations between different parameters of the sources are analysed in Sect. 3, while the results are discussed and summarised in Sect. 4.

2. The data

2.1. Giant-sized radio galaxies

The sample consists of 28 giant-sized galaxies out of the 36 the sources presented in Paper II, and 15 of 18 giant radio sources selected from the paper of Machalski et al. (2004). The redshift range of the sample sources is $0.06 < z < 0.82$ with a median value of 0.26 ± 0.03, and mean deviations from the median of -0.10, $+0.21$ (concerning an asymmetrical distribution). The 1.4-GHz luminosity $P_{1.4}[{\rm W\,Hz^{-1}}]$ has log values in the range $24.3 < \log P_{1.4} < 27.3$ with a median of 25.6 ± 0.07 and mean deviations of -0.43, $+0.47$. For all these 43 sources their geometry, radio spectrum, lobe brightness, arm ratio, core prominence, and equipartition energy density, internal pressure and magnetic field strength are homogeneously determined. 17 of the above 43 galaxies form the giant subsample, for which polarisation and

depolarisation parameters are available from Paper II. For simplicity, giant radio galaxies are referred to hereafter as GRGs.

2.2. Normal-sized galaxies

The comparison sample consists of 75 FRII-type sources for which the published data allowed a determination of the same parameters as for the sample of giant radio galaxies. The sources are selected to fulfil the following criteria:
– have the radio core detected;
– asymmetries in their arm-ratio, and luminosity and spectral index of the lobes, can be determined from the published maps;
– polarisation data are available in some cases.
As a result, the sample comprises (i) high-luminosity low-redshift 3CR sources selected from the papers of Leahy & Perley (1991), and Hardcastle et al. (1998); (ii) high-luminosity high-redshift 3CR, as well as low-luminosity low-redshift B2 sources used by Machalski et al. (2004) as a comparison sample for their giant radio galaxies sample. Since the desired polarisation data are limited to a fraction of these sources only, we include also; (iii) southern radio galaxies selected from the Molonglo survey by Ishwara-Chandra et al. (1998). The latter galaxies are chosen mostly for their polarisation and depolarisation data given in that paper. The redshift range in our comparison sample is $0.03 < z < 1.8$ with a median value of 0.26 ± 0.05, and the mean deviations from the median of -0.14, $+0.55$. The 1.4-GHz (log) luminosity range is $24.3 < \log P_{1.4}[\mathrm{W\,Hz^{-1}}] < 28.6$. A median value of the distribution is 26.8 ± 0.02, and mean deviations of -1.0, $+1.0$. For 47 of the 75 sources the polarisation and depolarisation parameters, similar to those in the GRG sample, were available from Garrington et al. (1991), Ishwara-Chandra et al. (1998), and Goodlet et al. (2004). Hereafter normal-sized radio galaxies are referred to as NSGs.

3. The analysis and results

3.1. The method

The aim of our analysis is to investigate any trends and/or correlations between physical parameters determined for the sample sources and the "fundamental" parameters: the redshift, z, radio luminosity at 1.4 GHz, $P_{1.4}$, and the linear size, D. The method applied in the present study is based on the homogeneous determination of a number of observational and physical parameters (m) for all (N) members of both samples, and then inserting these into a numerical array of $m \times N$ elements. Most of these parameters are interdependent, hence each parameter of the sample sources correlates somehow with the other parameters. Therefore, given the array, a statistical test for correlations between two variables in the presence of one or two other variables is used to examine relations among the properties of giant and normal-sized radio galaxies. In order to determine which correlation is the strongest, whether a third (or a third and a fourth) variable causes the correlation between the other two, and whether there is a residual correlation between these two variables when the third (or the third and fourth) is (are) held constant, we calculate the Pearson partial correlation coefficients for the correlation between the selected parameters.

Due to the fact that many correlations between different parameters seem to follow a power law, two numerical arrays are used: the first with primary values of some of these parameters, and the other with their logarithms. For example: D[kpc] and $1 + z$ are in the first array; $\log(D[\mathrm{kpc}])$ and $\log(1 + z)$ are in the other. Hereafter r_{XY} denotes the correlation coefficient for the correlation between parameters X and Y (hereafter referred to as the "direct" correlation), $r_{XY/U}$ is the partial correlation coefficient between these parameters in the presence of a third parameter, U, which can correlate with both X and Y, and $\mathcal{P}_{XY/U}$ is the probability that the test pair X and Y is uncorrelated when U is held constant. Similarly, $r_{XY/UV}$, $\mathcal{P}_{XY/UV}$ is the correlation coefficient for a correlation involving four parameters, and the related probability, respectively.

Table 1. The correlation of core (log) luminosity P_5^{c} with $P_{1.4}$, or $1 + z$, or D when other parameters are held constant.

Correlation $N = 118$	r_{XY}	$r_{XY/U}$ $r_{XY/V}$	$\mathcal{P}_{XY/U}$ $\mathcal{P}_{XY/V}$	$r_{XY/UV}$ $\mathcal{P}_{XY/UV}$
P_5^{c}–$P_{1.4}/D$	+0.703	+0.711	$\ll$0.0001	
P_5^{c}–$P_{1.4}/1+z$		+0.537	$\ll$0.0001	
P_5^{c}–$P_{1.4}/D$, $1+z$				+0.570 $\ll$0.0001
P_5^{c}–$(1+z)/P_{1.4}$	+0.538	+0.021	0.82	
P_5^{c}–$(1+z)/D$		+0.518	$\ll$0.0001	
P_5^{c}–$(1+z)/P_{1.4}$, D				+0.006 0.95
P_5^{c}–$D/P_{1.4}$	−0.172	+0.226	0.015	
P_5^{c}–$D/1+z$		−0.016	0.86	
P_5^{c}–$D/P_{1.4}$, $1+z$				+0.225 0.015

3.2. Radio core properties

In this subsection, we analyse the Pearson partial correlations between each of two radio core parameters: the core power and the core prominence, and other parameters of the sample sources which give the highest r_{XY}. A useful measure of the core prominence is the ratio $c_{\mathrm{p}} = S_{\mathrm{core}}/(S_{\mathrm{total}} - S_{\mathrm{core}})$ (cf. Morganti et al. 1993). Similarly to Lara et al. (2004), we derive this parameter using S_{core} measured at 5 GHz and S_{total} at 1.4 GHz.

3.2.1. The core power partial correlations

The strong correlation between the core power at 5 GHz and the total power at lower frequencies in the population of classical double radio sources is very well known (cf. Giovannini et al. 2001). This correlation can be attributed to the Doppler beaming of a parsec-scale jet (e.g. Bicknell 1994; Komissarov 1994) not discerned from the core with a medium (VLA) angular resolution, and can reflect different inclination angle of the nuclear jets, and thus the inclination of the entire radio source's axis to the observer's line of sight. In this case, relatively stronger cores should be observed in more strongly projected sources. Therefore, in giant radio galaxies, with the inclination angle very likely close to 90°, one could expect to observe relatively weaker cores which is not the case (cf. Lara et al. 2004).

Our data support the previous results, and we find that the direct correlation coefficient between $\log P_5^{\mathrm{core}}$ and $\log P_{1.4}$ is high. Nevertheless, the core power in our samples also correlates with other physical parameters; in order of decreasing r_{XY}: the redshift and linear size of the source, D. The partial correlation coefficients in the correlation of $\log P_5^{\mathrm{core}}$ with $\log P_{1.4}$, $\log(1 + z)$, and $\log D$ together with the related probabilities of their chance correlation are given in Table 1.

The above tests confirm the strong $\log P_5^{\mathrm{core}} - \log P_{1.4}$ correlation, and completely exclude any significant dependence of the core power on redshift, when $P_{1.4}$ and D are held constant.

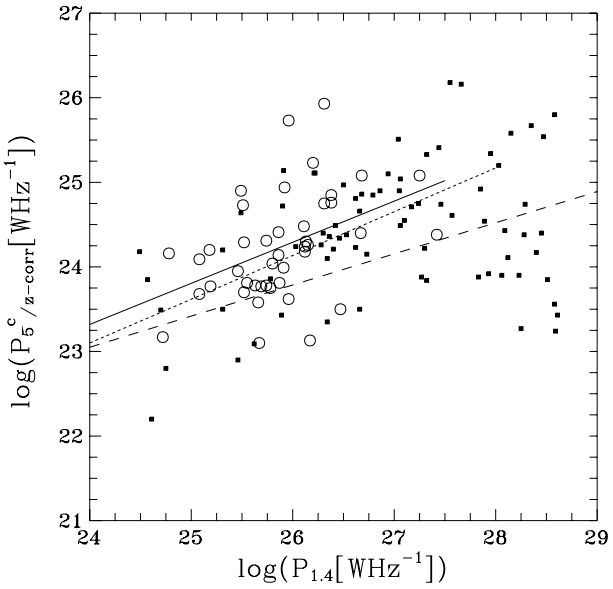

Fig. 1. Core power at 5 GHz transformed to the reference redshift of 0.5 vs. total power at 1.4 GHz. GRGs are marked with open circles and NSGs with small squares. The solid line indicates a least squares fit to the GRGs data. The dashed line shows the fit to the NSGs data, and the dotted line – the fit to the NSGs with the same luminosity range as the GRGs.

Fitting a surface to the values of $\log P_5^{\rm core}$ over the $\log P_{1.4}$–$\log(1+z)$ plane (where $P_{1.4}$ is in W Hz^{-1}), we found

$$P_5^{\rm core} \propto P_{1.4}^{0.55\pm0.08}(1+z)^{0.29\pm0.08}. \quad (1)$$

Note that the power of 0.55 is lower than that in the Giovannini et al.'s relation transformed to the cosmological constants adopted in this paper, $P_5^{\rm core} \propto P_{\rm t}^{0.60\pm0.04}$ (cf. Paper II), and Giovannini et al. do not take into account the dependence of the total power $P_{\rm t}$ on redshift.

Using Eq. (1) we eliminate dependence of the core power on redshift transforming its values to a reference value of z. The plot of $\log P_5^{\rm core}$ transformed to $z = 0.5$ as a function of $\log P_{1.4}$ is shown in Fig. 1. The sample GRGs are indicated by open circles, and the NSGs by small full squares. The solid and dashed lines show formal linear regressions of $\log P_5^{\rm core}$ on the $\log P_{1.4}$ axis for GRGs and NSGs, respectively. Although these regression lines suggest a trend of the GRGs cores to be more powerful as compared with the NSG cores of the same total radio power $P_{1.4}$, statistical tests indicate that differences between both the slopes and the $P_5^{\rm core}$ intercepts are statistically insignificant. The probability of being drawn from the same general population is between 40% and 60%. The difference between these regression lines almost disappears when NSG and GRG galaxies within the same total power range are compared, as indicated by the dotted line for the NSGs with $P_{1.4} < 10^{27.3}$ W Hz^{-1}.

3.2.2. The core prominence partial correlations

The correlation coefficients in the correlations of $c_{\rm p}$ with the source fundamental parameters indicate strong (by definition) anticorrelation with the source power $P_{1.4}$, and strong correlation with its size D. However, we find that the core prominence most strongly (anti)correlates with the source surface brightness, defined here as $\mathcal{B} = P_{1.4}/(D^2/AR)$, where AR is the source (its cocoon) axial ratio (for its definition cf. Paper II), and the source size is given in metres.

Table 2. The correlation of core (log) prominence $c_{\rm p}$ with $\mathcal{B}$, or $P_{1.4}$, or $1+z$, when other parameters are held constant.

Correlation $N = 118$	r_{XY}	$r_{XY/U}$ $r_{XY/V}$	$\mathcal{P}_{XY/U}$ $\mathcal{P}_{XY/V}$	$r_{XY/UV}$ $\mathcal{P}_{XY/UV}$
$c_{\rm p}$–$\mathcal{B}/P_{1.4}$	−0.643	−0.315	<0.001	
$c_{\rm p}$–$\mathcal{B}/1+z$		−0.548	≪0.0001	
$c_{\rm p}$–$\mathcal{B}/P_{1.4}$, $1+z$				−0.313 <0.001
$c_{\rm p}$–$P_{1.4}/\mathcal{B}$	−0.560	−0.034	0.72	
$c_{\rm p}$–$P_{1.4}/1+z$		−0.419	<0.0001	
$c_{\rm p}$–$P_{1.4}/\mathcal{B}$, $1+z$				−0.043 0.64
$c_{\rm p}$–$(1+z)/\mathcal{B}$	−0.410	+0.040	0.67	
$c_{\rm p}$–$(1+z)/P_{1.4}$		+0.019	0.84	
$c_{\rm p}$–$(1+z)/\mathcal{B}$, $P_{1.4}$				+0.029 0.76

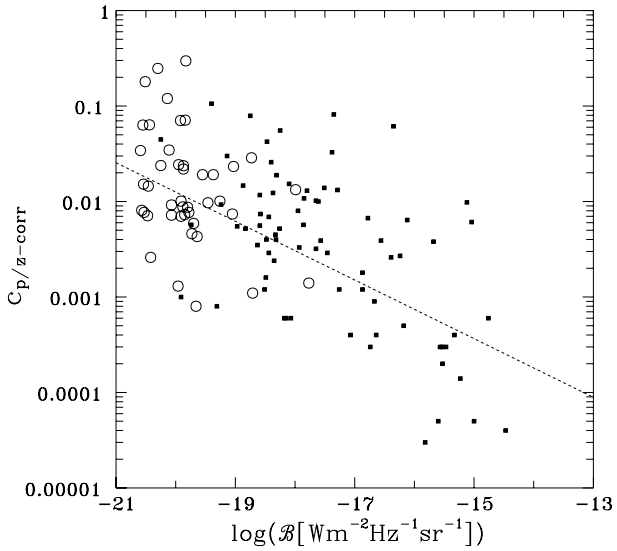

Fig. 2. Core prominence transformed to the reference redshift of 0.5 vs. source surface brightness. GRGs and NSGs are marked with the same symbols as in Fig. 1. The dashed line shows the least squares fit to the entire data.

The partial correlation coefficients in the correlation of $\log c_{\rm p}$ with $\log \mathcal{B}$, $\log P_{1.4}$, and $\log(1+z)$ together with the corresponding probabilities of their chance correlation are given in Table 2.

Whereas the core prominence most strongly correlates with the surface brightness, the partial correlation coefficients in Table 2 show that its dependences on the source's total power as well as on redshift are marginal when the surface brightness is kept constant. Fitting a surface to the values of $c_{\rm p}$ over the $\log P_{1.4}$–$\log(1+z)$ plane, we find

$$c_{\rm p} \propto P_{1.4}^{-0.23\pm0.05}(1+z)^{+3.00\pm0.35}. \quad (2)$$

The values of $\log c_{\rm p}$, transformed to $z = 0.5$ vs. $\log \mathcal{B}$ is presented in Fig. 2.

3.2.3. The core prominence and the orientation indicator

In the sample of Lara et al. (2004) comprising of large size FRI and FRII-type sources, the authors found an excess of sources with a core power larger than expected from their total power, and considered whether the ratio of $P_5^{\rm core}$ and $P_{\rm norm}^{\rm core}$, i.e. that calculated from the relation of Giovannini et al. (cf. Sect. 3.2.1),

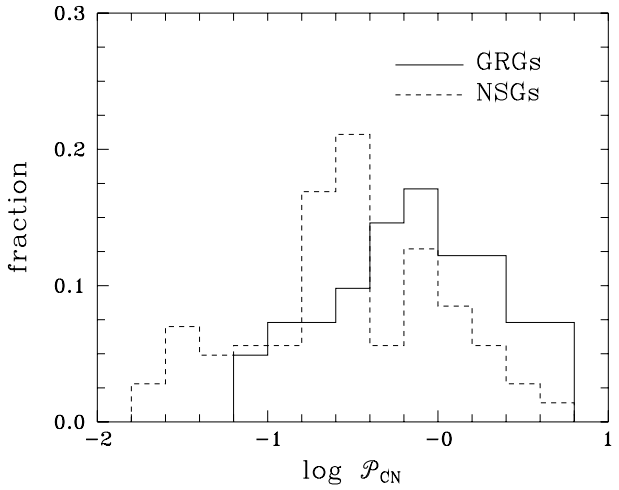

Fig. 3. Distribution of $\log \mathcal{P}_{CN}$ for the Giant (GRG: solid line) and "normal-size" (NSG: dashed line) radio galaxies.

might be an indicator of the source orientation angle ($\mathcal{P}_{CN}$ in their paper). For sources larger than 1 Mpc they found the median ratio of $\mathcal{P}_{CN} \approx 1.6$.

Our sample confirms the above effect, though qualitatively only. Using their normalization transformed to the cosmological constants adopted in our samples, the median of $\mathcal{P}_{CN}$ for GRGs and NSGs is $0.89^{+0.21}_{-0.13}$ and $0.29^{+0.04}_{-0.03}$, respectively. The distributions of $\log \mathcal{P}_{CN}$ for the sample GRGs and NSGs are shown in Fig. 3. A value of $\mathcal{P}_{CN} < 1$ for NSGs is justified because our comparison sample of radio sources does not include quasars, for which the core power is statistically higher than that for radio galaxies. On the other hand, the median of $\mathcal{P}_{CN}$ close to unity supports the result described in Sect. 3.2.1 that radio cores of giant-size radio galaxies are not statistically stronger than those for normal-size galaxies.

3.3. Equipartition energy density and magnetic field strength

Two other physical parameters of the sample sources derived directly from the observational data are: the equipartition energy density, u_{eq}, and magnetic field strength, B_{eq}. The values of these two parameters for the sample sources have been calculated using the formulae of Miley (1980), and assuming the ratio of energy in protons to that in electrons $k = 1$, and the filling factor $\eta = 1$ (cf. Paper II). Formally, we analyse relations of u_{eq} and B_{eq} with the sources' radio luminosity, size, and redshift. However, the equipartition energy density and corresponding magnetic field are related, by definition, to the luminosity and size with the canonical formulae $u_{eq} \propto P^{4/7}V^{-4/7}$ (i.e. $u_{eq} \propto P^{4/7}D^{-12/7}$), and $B_{eq} \propto u_{eq}^{1/2}$, respectively.

3.3.1. Energy density partial correlations

Our statistical analysis, involving the largest sources known, shows that besides the expected strong correlation between the energy density and the luminosity of sources, and anticorrelation with their size, there is also a significant direct correlation between this energy density and redshift. However, the size also anticorrelates with redshift, so we calculate the partial correlations between all these parameters. The Pearson partial correlation coefficients in the correlations between u_{eq}, $P_{1.4}$, D, and $1 + z$ are given in Table 3.

Table 3. The correlation of (log) equipartition energy density u_{eq} with $P_{1.4}$, or D, or $1+z$, when other parameters are held constant.

Correlation $N = 118$	r_{XY}	$r_{XY/U}$ $r_{XY/V}$	$\mathcal{P}_{XY/U}$ $\mathcal{P}_{XY/V}$	$r_{XY/UV}$ $\mathcal{P}_{XY/UV}$
$u_{eq}-P_{1.4}/D$	+0.866	+0.948	$\ll$0.0001	
$u_{eq}-P_{1.4}/1+z$		+0.765	$\ll$0.0001	
$u_{eq}-P_{1.4}/D, 1+z$				+0.897 $\ll$0.0001
$u_{eq}-D/L_{1.4}$	−0.802	−0.925	$\ll$0.0001	
$u_{eq}-D/1+z$		−0.830	$\ll$0.0001	
$u_{eq}-D/L_{1.4}, 1+z$				−0.925 $\ll$0.0001
$u_{eq}-(1+z)/D$	+0.631	+0.690	$\ll$0.0001	
$u_{eq}-(1+z)/P_{1.4}$		−0.059	0.55	
$u_{eq}-(1+z)/D, P_{1.4}$				+0.015 0.86

The partial correlations coefficients in Table 3 clearly exhibit a strong dependence of energy density (and so probably of average internal pressure) on both the total radio luminosity and the source's size. When these two parameters are kept constant, the apparent correlation between u_{eq} and redshift practically disappears. Some consequences of this effect are discussed in Sect. 4.

The direct correlation between u_{eq} and $(1 + z)$ in our sample is shown in Fig. 4a. The solid line indicates the presumed IGM pressure evolution in the form $p_{IGM} \propto u_{eq} \propto (1 + z)^5$. Fitting a surface to the values of $\log u_{eq}$ over the $\log P_{1.4}$–$\log D$ plane (where $P_{1.4}$ is in $\mathrm{W\,Hz^{-1}}$ and D in kpc), we find

$$u_{eq} \propto P_{1.4}^{0.65\pm0.03} D^{-1.33\pm0.05}. \quad (3)$$

The above relation does not differ much from that expected using the canonical formula. However, the difference between the powers of P and D can be real and justified by the non-constant axial-ratio parameter of the sources' cocoon, AR, and by the fact that P and D are not independent variables. Indeed, assuming that the values of both AR and D are a function of the source age, t, and taking $AR \propto t^{0.23\pm0.03}$ (Machalski et al. 2004) as well as $D \propto t^{3/(5-\beta)}$ with $\beta = 1.5$ (cf. Kaiser et al. 1997; Machalski et al. 2004), one can find $AR(D) \propto D^{0.27\pm0.03}$. Because the cocoon volume is $V \propto D^3AR^{-2}$, then $V^{-4/7} \propto D^{-1.4\pm0.1}$. Also as the luminosity of sources (according to all dynamical models) is time dependent, the power of $P_{1.4}$ in Eq. (3) may differ from the value of 4/7 if the samples comprise radio sources observed at different ages.

Using Eq. (3), we transform u_{eq} values (these values for the GRGs from our sample are given in Table 4 of Paper II, while those for the GRGs and NSGs from the sample of Machalski et al. (2004) are recalculated for $H_0 = 71\ \mathrm{km\,s^{-1}\,Mpc^{-1}}$ and $\Omega_m = 0.27$) to a reference 1.4-GHz luminosity of $10^{26}\ \mathrm{W\,Hz^{-1}}$ and size of 400 kpc. The relation between the transformed energy density and redshift of the sample sources with the regression line on the redshift axis is shown in Fig. 4b.

3.3.2. Magnetic field partial correlations

The Pearson partial correlation coefficients calculated for the correlations between the equipartition magnetic field strength, B_{eq} and the total radio luminosity, $P_{1.4}$, redshift, $1 + z$, and the source size, D, again confirm that the strongest (anti)correlation occurs between B_{eq} and D (logarithmic scales). For $N = 118$, the probability of a chance correlation is less than 0.0001.

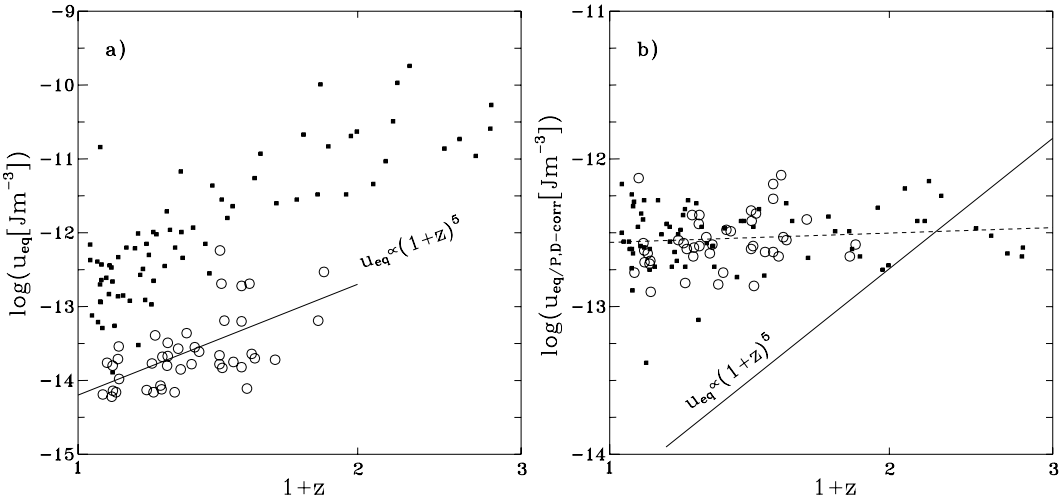

Fig. 4. a) Equipartition energy density vs. redshift, **b)** the same energy density transformed to the reference size of 400 kpc and 1.4-GHz total luminosity of 10^{26} W Hz^{-1}. GRGs and NSGs are marked with the same symbols as in Fig. 1. The solid line in **a)** and **b)** indicates the presumed IGM pressure evolution $p_{\rm IGM} \propto u_{\rm eq} \propto (1+z)^5$. The dashed line in **b)** shows the least squares fit to the transformed data.

Table 4. Example of the sample sources showing the correlation between $B_{\rm eq}$ and their age.

Source	D[kpc]	t[Myr]	$B_{\rm eq}$[nT]
3C 437	316	6.4	4.38
3C 322	283	7.3	3.28
3C 267	315	12	2.93
3C 244.1	294	14	1.72
3C 337	297	24	2.20
3C 357	296	27	0.60
3C 319	297	43	0.71
0828+324	296	59	0.24

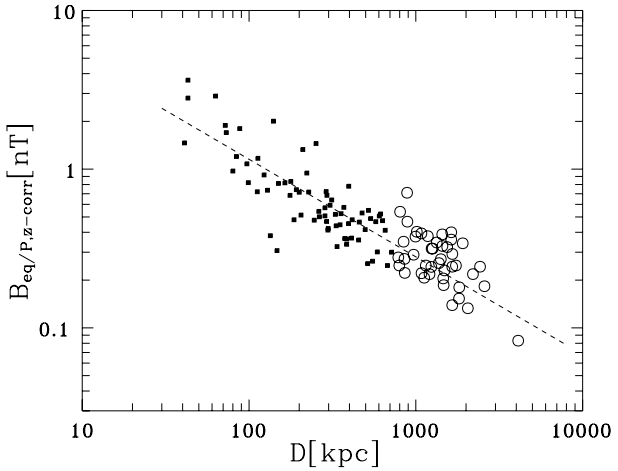

Fig. 5. Equipartition magnetic field strength, transformed to the reference 1.4-GHz luminosity of 10^{26} W Hz^{-1} and redshift of 0.5, vs. source size. GRGs and NSGs are marked with the same symbols as in Fig. 1. The dashed line indicates the least-squares fit to the transformed data.

As we did for the energy density parameter, a power-law dependence of $B_{\rm eq}$ on $P_{1.4}$, and $(1+z)$ values has been derived. Consequently $B_{\rm eq}$ values, transformed to the reference 1.4-GHz luminosity of 10^{26} W Hz^{-1} and redshift of 0.5, are plotted against source size (D) in Fig. 5. Though a dependence of the equipartition magnetic field on the source size is expected, we show this plot because, according to the dynamical model of Kaiser et al. (1997) and its application to observational data given in Machalski et al. (2004), it reflects a more fundamental dependence of the lobes' (or cocoon) energy density and the mean magnetic field strength on the dynamical age of radio sources. We would like to emphasize a partial dependence of some observational parameters of the sources, e.g. the total luminosity and size (referred here to as fundamental parameters), on their age. Besides, these two parameters depend also on the energy delivered to the lobes by the jets, as well as the density of the ambient environment. Though we are not able yet to determine that age for the entire sample of sources analysed in this paper, a subset of those sample sources with a very similar linear size of about 300 kpc, and different ages and equipartition magnetic fields, can be selected from Machalski et al. (2004). This subset is given in Table 4, where all columns are self-explanatory; the size D is recalculated using the cosmological constants applied in this paper. The entries in Table 4 clearly show the dependence of $B_{\rm eq}$ on the age, when D is held constant.

3.4. Polarisation and depolarisation characteristics

The rotation measure, *RM*, and depolarisation measure, *DP*, are closely related to the distribution of thermal plasma and magnetic fields both inside and outside the sources. The basic theory (Burn 1966; Gardner & Whiteoak 1966) predicts that a rotation of the polarisation plane without depolarisation would indicate a foreground-resolved Faraday screen, whereas a rotation accompanied by depolarisation would suggest a foreground screen as well as a screen local to the sources. In the sample of Goodlet & Kaiser (2005) (which constitute part of our NSGs sample) the authors found that both the measured dispersion of *RM* and the *DP* correlate with redshift concluding that their small-scale variations of *RM* are caused by a local screen.

Our analysis, based on the limited polarisation data for the GRGs sample taken at two frequencies only, does not allow convincingly constrain the location of possible screens. However, the correlation and partial correlation tests can show whether rotation and depolarisation properties of giant-sized and normal-sized radio galaxies are similar or not.

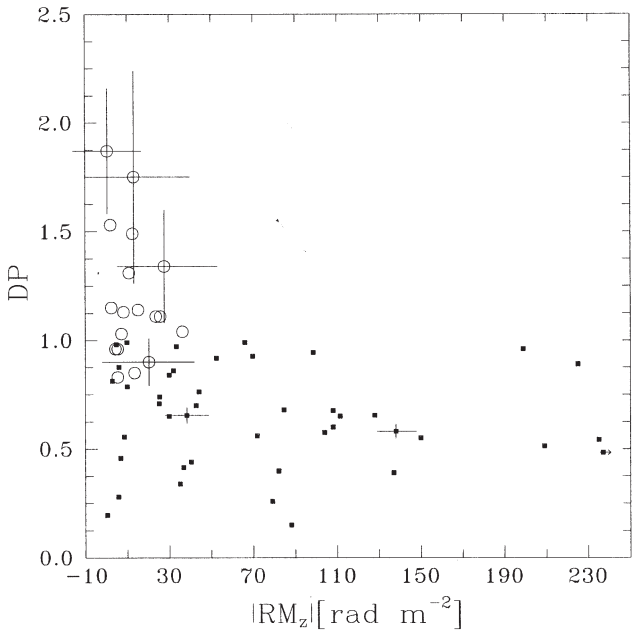

Fig. 6. Depolarisation measure vs. absolute value of rotation measure corrected for redshift, i.e. transformed to the sources' frame. Crosses show a typical error in both measures.

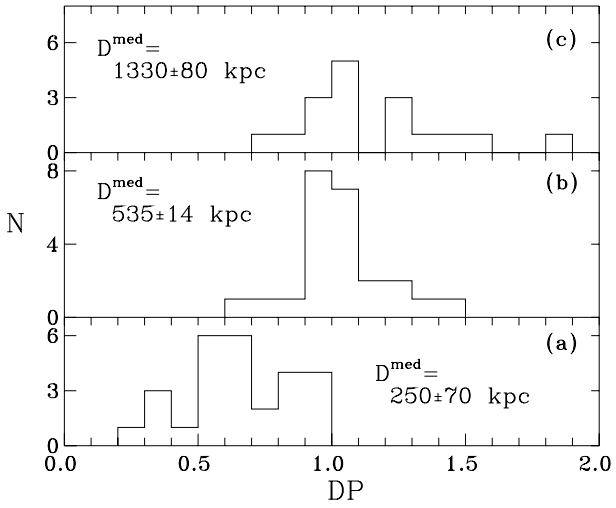

Fig. 7. Histograms of the depolarisation measure *DP* for **a)** radio galaxies from the samples of Garrington et al. (1991) and Goodlet et al. (2004); **b)** radio galaxies from the sample of Ishwara-Chandra et al. (1998); and **c)** giant radio galaxies from our sample.

3.4.1. Rotation measure partial correlations, and relation between rotation and depolarisation

The determination of the rotation measure, *RM*, and depolarisation measure, *DP*, for the sample GRGs was described in Paper II. The *RM* and *DP* values for the NSGs have been available only for the sample members studied by Garrington et al., and Goodlet et al. *RM* values are not available for the sources taken from Ishwara-Chandra et al., reducing our statistics to 44 sample sources with the rotation measure determined. For the partial correlation calculations, we take the average of the *RM* and *DP* values determined in the original papers for the lobes of the sample sources. The Pearson correlation coefficients and partial correlation coefficients for the correlation between *RM* and the sources' fundamental parameters show that the rotation measure is not correlated with any of the fundamental parameters, i.e. the redshift, radio luminosity, and size. Thus the *RM* values for the GRGs would support the conclusion drawn by Goodlet & Kaiser (2005) that most of the observed *RM* is caused by the Galactic magnetic field and not by a Faraday screen local to the sample sources.

However all sample sources are also depolarised. In principle, the measured depolarisation accompanied by a rotation of the polarisation plane can tell us something about the matter and magnetic fields in the source itself and/or between it and the observer. In practice, it is very difficult to recognize possible Faraday screens acting for a given radio source (cf. Laing 1984). Regardless of possible inner and/or outer screens, a decrease of depolarisation with λ^2 at short wavelengths should accompany an increase of rotation with λ^2.

The plot of *DP* vs. $|RM_z|$ (i.e. corrected to the sources' frame by multiplying the measured values by $(1+z)^2$) for the lobes of the sources with available *RM* values, shown in Fig. 6, indicates that the GRGs are, on average, less depolarised with the polarisation plane less rotated than the corresponding characteristics of the NSGs. This would suggest that the Faraday depth of intervening environment surrounding GRGs (their lobes or cocoon) is lower in comparison to that around less extended structure of NSGs. As the rotation and depolarisation measures are probably related, we analyse below how the *DP* values in our sample are correlated with the principal parameters, especially with the linear size.

Table 5. The correlation of depolarisation measure *DP* with (log) *D*, or $P_{1.4}$, or $1+z$, when other parameters are held constant.

Correlation $N = 64$	r_{XY}	$r_{XY/U}$ $r_{XY/V}$	$\mathcal{P}_{XY/U}$ $\mathcal{P}_{XY/V}$	$r_{XY/UV}$ $\mathcal{P}_{XY/UV}$
DP–$D/P_{1.4}$	+0.59	+0.47	<0.0001	
DP–$D/1+z$		+0.59	≪0.0001	
DP–$D/P_{1.4}$, $1+z$				+0.47 0.0002
DP–$P_{1.4}/D$	−0.41	−0.01	0.97	
DP–$P_{1.4}/1+z$		−0.45	0.0002	
DP–$P_{1.4}/D$, $1+z$				−0.16 0.61
DP–$(1+z)/P_{1.4}$	−0.15	+0.26	0.04	
DP–$(1+z)/D$		+0.14	0.27	
DP–$(1+z)/P_{1.4}$, D				+0.21 0.11

3.4.2. Depolarisation measure partial correlations

If the measured depolarisation, *DP*, or a part of it was caused by a screen local to the source, we would expect that *DP* may correlate with *D*. This is the case; the histograms of *DP* values in three ranges of *D* of the GRG and NSG radio galaxies investigated are shown in Fig. 7. Note that, according to the adopted definition of the depolarisation measure, an increase of the *DP* values means a decrease of the source's depolarisation. However, as the *DP* values can also correlate with the other fundamental parameters, we calculate the relevant Pearson correlation and partial correlation coefficients, and there are given in Table 5.

The above tests confirm a significant correlation of *DP* with *D*, and show a residual *DP*–log (1+*z*) correlation. Fitting a surface to the *DP* values over the log $P_{1.4}$–log (1+*z*) plane, we find

$$DP \propto P_{1.4}^{-0.23\pm0.06}(1+z)^{1.1\pm0.6}. \quad (4)$$

Table 6. Summary of the trends and correlations. The correlations are considered significant (Yes) if the probability of the observed result under the null hypothesis is <1%, marginally significant (Yes?) if it is <5%, and not significant (No) otherwise.

Dependence tested	Significant?
Core power is correlated with total radio luminosity	Yes (99.99%)
Core power is correlated with redshift	No
Core power in GRGs is higher than that in NSGs	No
Core prominence is correlated with total radio luminosity	No
Core prominence is correlated with redshift	No
Core prominence is correlated with surface brightness of the lobes or cocoon	Yes (99.9%)
Energy density is correlated with total radio luminosity	Yes (99.95%)
Energy density is correlated with redshift	No
Energy density is correlated with linear size	Yes (99.99%)
Energy density in GRGs is lower than that in NSGs	Yes (99.9%)
Equipartition magnetic field is correlated with linear size	Yes (99.99%)
Fractional polarisation in GRGs is lower than that in NSGs	No
Rotation measure in GRGs is lower than that in NSGs	?
Rotation measure is correlated with fundamental parameters (total radio luminosity, linear size, redshift)	No
Rotation measure is correlated with depolarisation	Yes?
Depolarisation measure is correlated with linear size	Yes (99.98%)
Depolarisation measure is correlated with redshift	No? (89%)

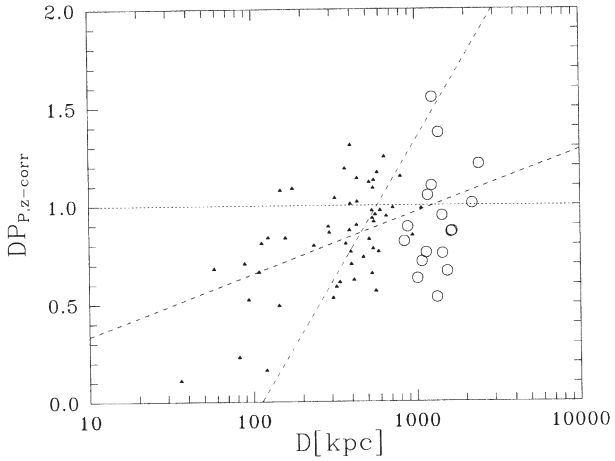

Fig. 8. Depolarisation measure between 1.4 GHz and 4.86 GHz vs. linear size of the sample sources. GRGs and NSGs are marked with the same symbols as in Fig. 1. The dashed lines indicate the least-squares linear regression of the data points on the abscissa and ordinate axes. The partial correlation coefficient $r_{DP,D/P,z}$ is +0.47 (cf. Table 5).

In spite of the very uncertain dependence of DP on $1 + z$ when $P_{1.4}$ and D are held constant, we transform the DP values into the reference values of $P_{1.4} = 10^{26.5}$ W Hz^{-1} and $z = 0.5$. The DP values corrected in this way are plotted against D in Fig. 8. As a result, larger radio galaxies tend to be less depolarised than smaller ones, suggesting again that their depolarisation may be caused by a thin IGM local to the sources. The statistical significance of this effect is very high (cf. Table 5).

4. Discussion of the results and conclusions

The important results of Sect. 3 are summarized in Table 6. In this section, we discuss some properties of the giant-size radio galaxies that have emerged from our analysis.

4.1. Core power and core prominence

The core power is highly correlated with the total radio luminosity of FRII-type radio sources, even if the influence of other fundamental parameters (the linear size and redshift) on the above correlation is eliminated. The core powers of GRGs do not differ from those of NSGs. However, the core prominence parameter does not depend on the total power, but anti-correlates with energy density in the lobes or cocoon of the sample sources. On the other hand, the energy density ought to evolve with the source age (cf. the dynamical models of Kaiser & Alexander 1997; Blundell et al. 1999; Manolakou & Kirk 2002). This implies that a dynamical age of the radio structure is a more fundamental parameter than its radio luminosity and size.

4.2. Energy density, internal pressure, and their implication for the hypothesis of the IGM pressure evolution with redshift

The former studies (e.g. Arnaud et al. 1984; Rawlings 1990) indicated that the minimum internal pressures in diffuse lobes and bridges of FRII-type radio galaxies equal the pressure of IGM in cases where detectable X-ray emitting gas surrounds the radio structure. Moreover, the studies also showed that the diffuse radio structures located outside these high-density environments may be in thermal equilibrium with the ambient medium whose emissivity cannot be directly determined. Therefore, the approximate equality of the derived internal and external pressures justifies the energy equipartition assumption that was, and is usually used in calculation of internal pressure within the radio lobes.

The expected electron pressure in the adiabatically expanding Universe is $p_{\rm IGM} = p^0_{\rm IGM}(1+z)^5$ with $p^0_{\rm IGM} = 2\times10^{-15}$ N m^{-2} (cf. Subrahmanyan & Saripalli 1993). On the other hand, analytical models of the dynamical evolution of FRII-type sources (e.g. Kaiser & Alexander 1997) assume that their internal pressure depends on the source's size, hence is a function of its age (cf. Eq. (2) in Kaiser 2000).

The statistical test in Sect. 3.3.1 shows that $u_{\rm eq}$ (thus likely the cocoon internal pressure) is independent of redshift when the radio luminosity and size are kept constant. If the tenuous material in the cocoon of GRGs attains an equilibrium state and its pressure equals the pressure of the IGM, the above result will disagree with the expected cosmological evolution of the IGM. Another possibility is that the cocoon, even in the largest sources, is still overpressed with respect to the surrounding medium. Therefore our result is identical with that of Schoenmakers et al. (2000), who concluded that there was no

evidence in their sample for a cosmological evolution of energy density in the lobes of GRGs, and there was therefore also no evidence for a cosmological evolution of pressure within the IGM. We also agree with their conclusion that a rejection of the hypothesis of the IGM pressure evolution proportional to $(1 + z)^5$ would be possible if high-redshift GRGs (at $0.6 < z < 1$) with energy densities less than about 2×10^{-15} N m^{-3} were discovered.

4.3. Polarisation

Global polarisation characteristics of the sample GRGs are similar to those of NSGs. The only trends (however of low statistical significance due to the low number of sources in the samples used) are:
– the dispersion of the rotation measure of GRGs is lower than that of NSGs; and
– GRGs tend to be less depolarised than NSGs.
Thus, taking also into account the significant correlation of the depolarisation measure with the source linear extent, all these characteristics suggest that a part of the rotation and depolarisation is caused by a Faraday screen local to the extragalactic FRII-type radio sources.

Because the low depolarisation and rotation measures determined for GRGs describe the polarised emission from their lobes, the above implies that the IGM surrounding the lobes (or cocoon) of GRGs is evidently less dense than that in a vicinity of NSGs. Obviously, these global characteristics, determined at two observing frequencies only, tell us nothing about the geometry and composition of the intervening material. Further analysis of polarisation asymmetries between the lobes can be more promising, which we intend to perform in a separate paper.

Acknowledgements. We are grateful to Dr Peter Barthel for constructive comments which helped us to improve the paper and clarify our results. This work was supported in part by the State with funding for scientific research in years 2005–2007 under contract No. 0425/PO3/2005/29

References

Arnaud, K. A., Fabian, A. C., Eales, S. A., et al. 1984, MNRAS, 211, 981
Bicknell, G. V. 1994, ApJ, 422, 542
Blundell, K. M., Rawlings, S., & Willott, C. J. 1999, AJ, 117, 677
Burn, B. J. 1966, MNRAS, 133, 67
Fanaroff, B. L., & Riley, J. M. 1974, MNRAS, 167, 31P
Hardcastle, M. J., Alexander, P., Pooley, G. G., & Riley, J. M. 1998, MNRAS, 296, 445
Gardner, F. F., & Whiteoak, J. B. 1966, ARA&A, 4, 245
Garrington, S. T., Conway, R. G., & Leahy, J. P. 1991, MNRAS, 250, 171
Giovannini, G., Cotton, W. D., Feretti, L., et al. 2001, ApJ, 552, 508
Goodlet, J. A., & Kaiser, C. R. 2005, MNRAS, 359, 1456
Goodlet, J. A., Kaiser, C. R., Best, P. N., & Dennett-Thorpe, J. 2004, MNRAS, 347, 508
Ischwara-Chandra, C. H., Saikia, D. J., Kapahi, V. K., & McCarthy, P. J. 1998, MNRAS, 300, 269
Kaiser, C. R. 2000, A&A, 362, 447
Kaiser, C. R., & Alexander, P. 1997, MNRAS, 286, 215
Kaiser, C. R., Dennett-Thorpe, J., & Alexander, P. 1997, MNRAS, 292, 723
Komissarov, S. 1994, MNRAS, 269, 394
Laing, R. A. 1984, in Physics of Energy Transport in Extragalactic Radio Sources, Proc. of NRAO Workshop No. 9, ed. A. H. Bridle, p. 90
Lara, L., Giovannini, G., Cotton, W. D., et al. 2004, A&A, 421, 899
Leahy, J. P., & Perley, R. A. 1991, AJ, 102, 537
Machalski, J., Jamrozy, M., & Zola, S. 2001, A&A, 371, 445 (Paper I)
Machalski, J., Jamrozy, M., Zola, S., & Koziel, D. 2006, A&A, 454, 85 (Paper II)
Machalski, J., Chyży, K. T., & Jamrozy, M. 2004, AcA, 54, 249
Manolakou, K., & Kirk, J. G. 2002, A&A, 391, 127
Miley, G. 1980, ARA&A, 18, 165
Morganti, R., Killeen, N. E. B., & Tadhunter, C. N. 1993, MNRAS, 263, 1023
Rawlings, S. 1990, Proc. 2nd Wyoming Conf., The Interstellar Medium in External Galaxies, ed. D. J. Hollenbach, & H. A. Thronson, 188
Schoenmakers, A. P., Mack, K.-H., de Bruyn, A. G., et al. 2000, A&AS, 146, 293
Subrahmanyan, R., & Saripalli, L. 1993, MNRAS, 260, 908